*How to Cite:* Galiyeva, A.R., Yessentayeva, N.A., Marsel, D.T., Daribay, A.T., Sadyrbekov, D.T., Moustafine, R.I., & Kutulutskaya, T.V. (2025). Polylactide Acid-Based Nanoparticles for Controlled Delivery of Isoniazid and Rifampicin: Synthesis, Characterization, and *In Vitro* Release Study. *Eurasian Journal of Chemistry, 30, 2(118), 95-108*. https://doi.org/10.31489/2959-0663/2-25-12

## CHEMICAL TECHNOLOGY

*Article*

Received: 28 February 2025 | Revised: 15 May 2025 |
Accepted: 22 May 2025 | Published online: 28 May 2025

UDC 66-971; 620.3

https://doi.org/10.31489/2959-0663/2-25-12

Aldana R. Galiyeva*[1], Nazgul A. Yessentayeva[1], Dias T. Marsel[1], Arailym T. Daribay[1], Daniyar T. Sadyrbekov[1], Rouslan I. Moustafine[2], Tatyana V. Kutulutskaya[3]

[1]*Karaganda Buketov University, Karaganda, Kazakhstan;*
[2]*Institute of Pharmacy, Kazan State Medical University, Kazan, Russia;*
[3]*"Regional Center of Phthisiopulmonology" of the Health Department of Karaganda region, Karaganda, Kazakhstan*
*(*Corresponding author's e-mail: aldana_karaganda@mail.ru)*

# Polylactide Acid-Based Nanoparticles for Controlled Delivery of Isoniazid and Rifampicin: Synthesis, Characterization, and *In Vitro* Release Study

The global problem of tuberculosis (TB) requires advanced drug delivery systems that improve treatment efficacy. In this study, polylactic acid (PLA)-based drug carriers were developed for the controlled delivery of the first-line anti-TB drugs isoniazid (INH) and rifampicin (RIF). The main objective of this study is to improve PLA-based NP formulations through optimization to achieve maximum drug content coupled with enhanced stability to improve treatment outcomes. PLA-RIF-INH nanoparticles (NPs) were prepared by double emulsion method using ultrasonic homogenizer, using different surfactants (polyvinyl alcohol, Tween-80 and Pluronic F-127) and with different organic solutions (dichloromethane, dimethyl sulfoxide and ethyl acetate) at different phase ratios. The produced NPs had an average size of 197±8 nm with a polydispersity index of 0.287±0.048 and contained 23±2 % INH and 20±8 % RIF for a NPs yield of 65±2 %. The release of drugs from PLA NPs was investigated using the flow cell method and the vertical diffusion method at different pH values simulating gastrointestinal conditions. It was shown that PLA-RIF-INH NPs have pronounced antimycobacterial activity against Mycobacterium tuberculosis H37Rv and isoniazid-resistant strain, which confirms the prospect of their use in tuberculosis therapy.

*Keywords*: drug delivery systems, nanoparticles, polylactic acid, anti-tuberculosis drugs, double emulsion, flow cell method, vertical diffusion method, Mycobacterium tuberculosis, ultrasonic homogenization



## *Introduction*

The development of advanced drug delivery systems becomes a crucial focus of pharmaceutical research, as they address infectious diseases, particularly tuberculosis (TB). The current standard formulations of drugs face multiple drawbacks when they are not properly absorbed in the body and are eliminated quickly, while causing unwanted side effects [1]. Colloidal drug delivery systems have become important due to their ability to improve drug solubility together with their protective effect on active pharmaceutical ingredients and controlled release capabilities. PLA serves as an outstanding biodegradable material for drug delivery applications due to its ability to create stable nanostructures and its notable properties of biocompatibility and biodegradability [2-3]. PLA-based colloidal systems maintain drug circulation times effectively while targeting delivery and reducing toxicity which makes them ideal to encapsulate anti-TB drugs [4].

This study investigates the synthesis and stability aspects of PLA-based colloids and presents the methods for incorporating essential tuberculosis drugs such as isoniazid and rifampicin. Rifampicin together with isoniazid operates as front-line tuberculosis drugs for widespread medical use in tuberculosis therapy [5]. The drugs provide effective tuberculosis treatment by restraining both Mycobacterium tuberculosis (MTB)

growth and multiplication. Despite their high success rate in treatment there exists a possible resistance development against these drugs, primarily because of inadequate treatment adherence and improper dosing schedule [6]. Multiple drugs are combined for treatment purposes when resistance emerges against one agent to control resistant bacterial strains effectively [7-8].

This investigation examines double emulsion techniques to develop precise drug delivery methods for anti-TB medications that focus on delivering these agents effectively to bacterial cells. The optimization procedure involved testing multiple factors which included selecting different organic solvents, various stabilizing surfactant concentrations, defining the ratio of organic to aqueous phase and using different molecular weights of polymers during nanoparticle formation. The drug release profiles alongside size and stability of nanoparticles depend strongly upon these particular factors. The study analyzes how PLA-based nanoparticles perform physically through size distribution assessments and surface morphology inspections and investigations of their stability in simulated body fluids. Scanning electron microscopy (SEM) was used to study morphological properties and additional characterization involved infrared spectroscopy (IR), thermogravimetric analysis (TGA), and differential scanning calorimetry (DSC) of the nanoparticles. In vitro experiments evaluated how drug substances released from polymer matrices at various time points. The study analyzes these characteristics to improve the PLA-based nanoparticle system with a more controlled drug release profile for better TB treatment results with drug-resistant strains.

## *Experimental*

### *Materials*

Poly (D,L-lactide) molecular weight (MW) 10,000, 15,000 and 20,000; Pluronic F-127 powder, Polyvinyl alcohol (PVA) (MW 9000–10,000, 80 % hydrolyzed); isoniazid with an in-medical purity of over 99 %, rifampicin with indicated purity over 99 %; dimethyl sulfoxide (DMSO) (≥99.5); ethyl acetate (EA) (≥99.5); dichloromethane (DCM) (≥99.5) were purchased from Sigma Aldrich (St. Louis, MO, USA). Tween 80 solution was purchased from CJSC "Kupavnareaktiv" (Russia, Old Kupavna city).

### *Preparation of PLA-RIF-INH NPs*

Nanoparticles of PLA-RIF-INH were prepared by double emulsion method [9–11]. A solution of INH drug substance (at a concentration of 2–10 mg/mL) dissolved in 1 mL water was combined with 5 mL of PLA solution in organic solvent for the synthesis. The hydrophobic RIF (at a concentration of 2–10 mg/mL) substance needed separate dissolution in an organic solvent and water mixture before addition to PLA solution in the same organic solvent. A primary emulsion formed due to mixing those components after which an ultrasonic homogenizer (Bandelin Sonopuls HD 2070, Bandelin Elec., Germany) ran the mixture continuously for two minutes. A primary emulsion received 10 mL of aqueous phase which included stabilizer (PVA, Tween-80, Pluronic F-127) as a surfactant through droplet addition. An ultrasonic homogenizer stabilized a secondary emulsion from the combined solution. A magnetic stirrer operated at room temperature under stirring for 6 hours to evaporate the solvent from this emulsion. The separation of RIF and INH-loaded PLA nanoparticles occurred through a centrifugation process at 14000 rpm for 30 minutes.

### *Determination of Particle Size, Polydispersity and ζ-potential of PLA-RIF-INH NPs*

The Zetasizer Nano S90 (Malvern Instruments Ltd., Malvern, UK) measured the nanoparticle size distribution and polydispersity index through Dynamic Light Scattering (DLS) examinations. The nanoparticle size examination required 5–8 drops of nanoparticles added to 1.5–2 mL of distilled water. The measurement of the samples took place at 25 °C while using a 90° scattering angle for detection. The ζ-potential was measured with a ζ-potential analyser (NanoBrook ZetaPALS, Holtsville, NY, USA) using electrophoretic laser Doppler anemometry. The analysis with scanning electron microscopy (SEM) evaluated the dimensions together with surface structures and shapes of the nanoparticles. A MIRA 3 LM TESCAN (Brno, Czech Republic, EU) served for SEM analysis.

### *Evaluation of Drug Loading Efficiency and Nanoparticles' Yield*

The determination of drug loading in polymer matrices relied on drug detection from unincorporated drug concentrations in the supernatant. The quantification method used HPLC along with a Shimadzu LC-20 Prominence system featuring a Shimadzu Scientific Instruments UV/VIS detector. Acetonitrile and water (60:40) formed the mobile phase which ran at 0.8 mL/min through the system. The Promosil C18 column from Agilent Technologies (Tokyo, Japan) operated for component separation with a 5 μm sorbent grain size

and 100 Å pore size within 4.6 × 150 mm dimensions. Raising the column temperature to 40 °C served as the maintenance condition. The injection used 10 μL sample with loop injection. The calculations for drug loading efficiency were made using the following formula:

$$\text{Loading efficiency}\left(LE, \%\right) = \frac{\text{Total mass of drug} - \text{mass of free drug}}{\text{Mass of } NPs} \times 100\ \%;$$

$$\text{Nanoparticles yield}\left(\%\right) = \frac{\text{Mass of } NPs}{\text{Total mass of drug} + \text{mass of } PLA} \times 100\ \%.$$

*In Vitro Drug Release from PLA-RIF-INH NPs*

For the investigation of in vitro drug release two analytical approaches were applied: the Flow-Through Cell apparatus with CE 7Smart technology from Sotax (Aesch, Switzerland) and vertical delivery through Franz PHOENIX™ DB-6 cells from Telodyne Hanson Research (Chatsworth, GA, USA) [9, 10]. The investigation applied phosphate buffer solutions at three pH values to replicate physiological conditions: pH 1.2 for gastric conditions and pH 6.8 for intestinal conditions alongside pH 7.4 for blood plasma conditions. Each solution operated at 37 ± 0.5 °C during testing.

The CE 7Smart instrument operated at a continuous flow rate of 2 mL/min during Flow-Through Cell method testing. The experiments employed Float-A-Lyzer® G2 nanoadapters (Merck KGaA, Darmstadt, Germany) as the dialysis membrane with known pore sizes within the range of 8000 to 10,000 Da. The experiment lasted for 24 hours.

In the vertical diffusion method using the Franz cell employed dialysis membranes (MWCO = 8000 Da, Medicell International Ltd., London, UK) were placed the polymeric nanoparticles loaded anti-tuberculosis drugs at 200 rpm stirring. The experimental duration spanned across 48 hours. The collected release medium samples underwent UV/V is spectrophotometer (Lambda 25, PerkinElmer, Waltham, MA, USA) analysis at 475 nm wavelength for RIF and 254 nm wavelength for INH at predefined measurement times of 0.5, 1, 2, 4, 8, 24 and 48 hours. Fresh medium replaced the withdrawn samples at each measurement point. A calibration curve containing drug solutions at specific concentrations served as the comparison standard for analyzing the collected data. A mathematical formula served to calculate the drug release speed in this experiment:

$$\text{Drug release}\left(\%\right) = \frac{\text{Mass of released drug}}{\text{Mass of total drug in nanoparticles}} \times 100\ \%.$$

*Thermal Analysis Using Thermogravimetry and Differential Scanning Calorimetry*

TGA and DSC measurements were carried out on a LabSYS evo TGA/DTA/DSC analyzer (Setaram, Caluire France) [12–14]. The experiment took place between 30 °C and 550 °C. A controlled heating process at 10 °C/min was performed while the samples were put inside an aluminum oxide crucible. Under a nitrogen atmosphere the analysis proceeded with a continuous gas flow of 30 mL/min.

*Infrared Spectroscopic Analysis of PLA-RIF-INH NPs*

The FSM 1202 spectrometer (Infraspek Ltd., Russia) determined the characteristics of the prepared nanoparticle samples through IR spectroscopy tests [15, 16]. The potassium bromide (KBr) pellet technique recorded the Fourier-transform infrared (FTIR) spectrum data. A pellet was made from blending 3 mg of the sample with 100 mg of KBr using pellet formation methods. A spectral analysis covered the wavelength span from 4000 to 400 $cm^{-1}$.

*In vitro Evaluation of Antimycobacterial Activity of PLA-RIF-INH Nanoparticles*

In vitro tests were conducted under sterile conditions using Airstream AC2-4E8 biosafety cabinets (Esco Micro Pte. Ltd., Singapore), which ensured a contamination-free environment through negative pressure and HEPA filtration. The antimycobacterial efficacy of PLA-RIF-INH nanoparticles was assessed using three MTB strains: the drug-sensitive H37Rv strain, an isoniazid-resistant strain (H), and a rifampicin-resistant strain (R). Nanoparticles were tested at concentrations corresponding to 8 mg/mL of rifampicin and 8 mg/mL of isoniazid. The bacteriostatic activity of the nanoparticles was determined by evaluating MTB growth on Levenstein-Jensen solid medium [17–19]. Inoculated tubes were incubated for 4 weeks, after which the number of colony forming units (CFUs) was recorded. Antimicrobial activity was assessed by comparing CFU counts between treated samples and controls. Positive cultures were stained using the Ziehl–Neelsen method [20], and the stained smears were subsequently examined with a Leica DMLS microscope.

*Statistical Analysis*

The research data represent mean ± standard deviation while statistical analysis through Minitab 19 Statistical Software implemented one-way analysis of variance (ANOVA) to determine group difference significance.

## *Results and Discussion*

The double emulsion method is an effective technique for creating nanoparticles based on polymers, including PLA, according to the literature [9–11]. This encapsulation method provides highly efficient ways to incorporate both hydrophobic and hydrophilic substances into drug delivery systems. Obtaining a double emulsion starts by mixing the active ingredients as an aqueous emulsion with an organic solution protected by stabilizing agents. When the second emulsion is formed, it is converted into stable nanoparticles after evaporation of the solvent [21]. The novelty of this work is the use of ultrasonic homogenizer to enhance emulsion formation by double emulsion method to produce PLA-RIF-INH NPs (Figure 1). The ultrasonic treatment improves dispersing the active ingredient particles in the polymer matrix, resulting in improved distribution uniformity and higher encapsulation standards. This innovative approach allows the production of smaller nanoparticles, contributing to the clarification of their morphological characteristics.

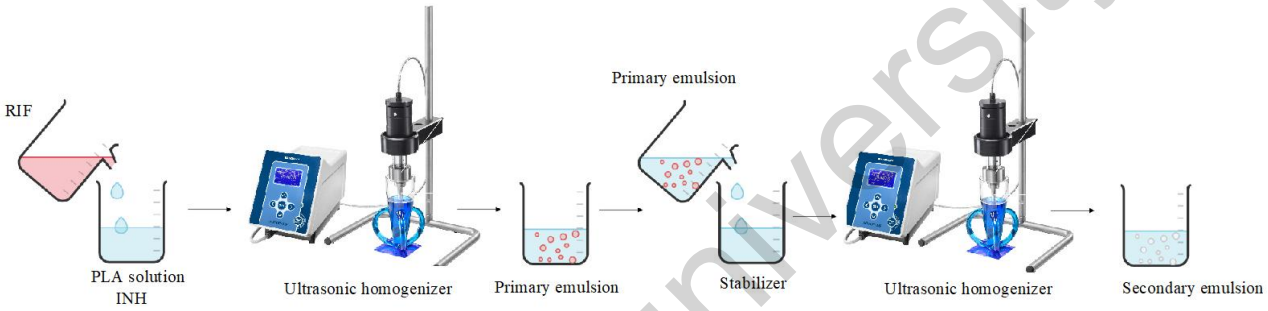


Figure 1. Scheme for producing PLA-RIF-INH NPs by double emulsion method

An appropriate choice of organic solvent stands as a vital component in double emulsion solvent evaporation because it controls nanoparticle formation along with their stability and drug entrapment capacity. For proper drug dispersing within the polymer matrix the solvent needs to demonstrate appropriate solubility toward hydrophilic and hydrophobic elements. The emulsifying capacity must be strong because emulsion stability depends on it, which affects nanoparticle size, dispersity, and drug loading efficiency. The present work investigated the three different organic solvents DCM, DMSO and EA to study their effects on the physicochemical features of PLA-based nanoparticles [16]. The formation process of nanoparticles gets substantially affected by the different physicochemical properties found in three solvents including volatility, solubility and miscibility with aqueous phases. Results on the influence of organic solvents on physical and chemical properties of nanoparticles are presented in Table 1.

Table 1

**Effect of organic solvents on physicochemical properties of PLA-RIF-INH NPs**

| Organic solvent | Average size of NPs, nm | PDI | LE (INH), % | LE (RIF), % | NPs yield, % |
|---|---|---|---|---|---|
| DCM | 365±2 | 0.060±0.002 | 26±4 | 26±5 | 24±5 |
| DMSO | 545±4 | 0.422±0.035 | 10±7 | 10±7 | 11±2 |
| EA | 314±5 | 1.000±0.102 | 19±5 | 19±5 | 16±9 |

Among the solvent systems tested, DCM provided the most favorable results for the formation of nanoparticles. The size of the nanoparticles produced was 365±2 nm, and the lowest PDI was found to be 0.060±0.002, indicating a highly homogeneous distribution of nanoparticles, which is a desirable property for drug delivery applications. In fact, not only was DCM found to yield highly uniform sized nanoparticles, but it was also the most efficient solvent system in terms of drug loading: the LE was measured at 26±4 % for INH and 26±5 % for RIF, with a yield of 24±5 % for the nanoparticles themselves. DMSO produced opposite results: the size was large (545±4 nm), the PDI was high (0.422±0.035), signifying polydispersity, and

the LE was actually quite low (10±7 %) for both antitubercular medications; the yield of the DMSO nanoparticles was 11±2 %, as well. EA had intermediate size results, but it was found to be the least stable solvent system, with the highest sharp distribution of sizes: the PDI registered was 1.000±0.102. The results demonstrate that DCM represents the optimal solvent for producing PLA-based nanoparticles because it generates uniform tiny particles with better drug loading along with high yield values. Both DMSO and EA do not attain satisfactory laboratory outcomes as nanoparticle formulations and exhibit elevated polydispersity indices because of their limited effectiveness in solvent performance.

Studies on nanoparticle synthesis with organic solvents requires additional attention to surfactants because these molecules are essential for stabilizing nanoparticles while influencing their characteristics. Results provided in Table 2 summarize the obtained data.

Table 2

**Effect of different surfactants on the characteristics of PLA-RIF-INH NPs**

| Surfactant | Average size of NPs, nm | PDI | LE (INH), % | LE (RIF), % | NPs yield, % |
|---|---|---|---|---|---|
| PVA | 354±2 | 0.072±0.025 | 23±4 | 26±5 | 54±7 |
| Tween-80 | 486±3 | 0.234±0.033 | 29±5 | 30±2 | 40±5 |
| Pluronic F-127 | 534±2 | 0.495±0.047 | 13±6 | 13±7 | 8±7 |

The synthesis process of PLA-RIF-INH nanoparticles is directly influenced by the type of surfactant selected. PVA resulted in creating the nanoparticles with the smallest average size, whereas nanoparticles produced with Pluronic F-127 and Tween-80 became larger in size. The synthesis of PLA-RIF-INH nanoparticles with a PVA-based surfactant results in the most uniform particle size distribution, as indicated by the lowest polydispersity index compared to Pluronic F-127 and Tween-80, which show higher polydispersity. Tween-80 serves as the most effective surfactant for drug loading as it yields in 29±5 % INH and 30±2 % RIF, but Pluronic displays low values of loading (?) at 13±6 % INH and 13±7 % RIF. The drug loading efficiency of INH and RIF using PVA stands at 23±4 % and 26±5 % respectively. The NPs yield reached 54±7 % through the use of PVA which made it the optimal surfactant choice for the manufacturing process. The NPs yield reaches 40±5 % and 8±7 % when using Tween-80 and Pluronic. The selection of surfactant serves as a critical factor during PLA-RIF-INH NPs synthesis, as PVA delivers the best outcomes regarding size control together with uniform distribution and drug loading capacity and particle yield. Our analysis focuses on the impact of PVA concentration on essential features that define the created nanoparticles (Table 3).

Table 3

**Effect of PVA concentration on the characteristics of PLA-RIF-INH nanoparticles**

| PVA concentration, % | Average size of NPs, nm | PDI | LE (INH), % | LE (RIF), % | NPs yield, % |
|---|---|---|---|---|---|
| 0.3 | 658±5 | 0.160±0.015 | 6±3 | 5±6 | 45±3 |
| 0.5 | 367±8 | 0.127±0.023 | 23±4 | 26±5 | 44±1 |
| 1 | 287±8 | 0.358±0.054 | 10±2 | 10±2 | 61±5 |
| 1.5 | 190±7 | 0.219±0.047 | 25±6 | 29±8 | 67±4 |
| 3 | 127±3 | 0.363±0.046 | 16±5 | 17±3 | 60±8 |

The particle size of nanoparticles becomes smaller when PVA concentration rises. The size of the nanoparticles decreases from 658±5 nm to 127±3 nm when PVA concentration increases from 0.3 % to 3 %. Nanoparticle Polydispersity Index depends on the concentration of Polyvinyl Alcohol present in the formulation. The best particle size distribution is achieved at a PVA concentration of 0.5 %, where the PDI reaches 0.127±0.023. PDI shows increased variations at PDI concentrations of 1 % and 3 % because these levels cover a wider range of particle dimensions. The incorporation amounts of INH and RIF in the nanocarriers show a direct relationship with PVA concentration values. At PVA concentration of 1.5 % both INH and RIF achieve their highest loading efficiency to reach 25±6 % and 29±8 % respectively. The optimal stabilization of the emulsion and suitable drug encapsulation conditions within nanoparticles occur at this specific surfactant concentration of 1.5 %. The nanoparticle producing process depends directly on how much PVA solu-

tion is used. The maximum INH and RIF loading efficiency together with the highest nanoparticle yield (67±4 %) occur when the PVA concentration reaches 1.5 %. The nanoparticle yield decreases slightly at 0.3 % and 0.5 % PVA concentrations although the size and PDI values remain relatively good. A 1.5 % PVA concentration functions as the optimal condition for making PLA-RIF-INH NPs because it produces the most desirable particle size together with the highest drug loading ratio and nanoparticle yields.

Different molecular weights of PLA were used to study the relationship between nanoparticle parameters, such as particle size, polydispersity, drug loading efficiency, and yield (Table 4).

Table 4

**Effect of polymer molecular weight on PLA-RIF-INH NPs characteristics**

| Molecular weight of PLA | Average size of NPs, nm | PDI | LE (INH), % | LE (RIF), % | NPs yield, % |
|---|---|---|---|---|---|
| 10 000 | 138±4 | 0.251±0.017 | 79±2 | 1±2 | 37±5 |
| 15 000 | 197±8 | 0.287±0.048 | 23±2 | 20±8 | 65±2 |
| 20 000 | 263±4 | 0.340±0.019 | 11±4 | 11±3 | 43±2 |

The highest INH loading efficiency of 79±2 % was achieved using PLA with MW 10000 for the formation of particles with 138±4 nm dimensions and PDI 0.251±0.017 yet the nanoparticles' yield reached only 37±5 %. PLA 15,000 produced nanoparticles with 197±8 nm dimensions along with 23±2 % INH content but achieved 20±8 % RIF content and reached exceptional nanoparticles' yields at 65±2 %. The increase in molecular weight to 20,000 resulted in nanoparticle sizes of 263±4 nm while the PDI rises to 0.340±0.019 and INH and RIF loading efficiency decreases to 11±4 % and 11±3 % producing a nanoparticle yield of 43±2 % at this molecular weight.

The study evaluated the effect of different concentrations of INH and RIF loaded in polymeric nanoparticles. Optimization of the elements can improve system stability and loading efficiency while maintaining controlled drug release. The selection process for INH and RIF concentrations should focus on optimizing loading efficiency while ensuring both small particles and narrow size distribution. The results are summarized in Table 5.

Table 5

**Effect of drug concentration on PLA-RIF-INH NPs characteristics**

| Concentration of INH, mg/mL | Concentration of RIF, mg/mL | Average size of NPs, nm | PDI | LE (INH), % | LE (RIF), % | NPs yield, % |
|---|---|---|---|---|---|---|
| 2 | 2 | 263±3 | 0.224±0.059 | 9±2 | 10±2 | 30±4 |
| 4 | 4 | 257±4 | 0.287±0.048 | 23±2 | 20±6 | 37±8 |
| 8 | 8 | 266±1 | 0.196±0.061 | 14±7 | 15±3 | 78±4 |
| 10 | 10 | 259±2 | 0.146±0.035 | 2±6 | 3±4 | 18±2 |

When the drug concentration reaches 2 mg/mL the NPs have an average diameter of 263±3 nm and a polydispersity of 0.224±0.059 which points on a uniform particle distribution. The achieved drug loading efficiency percentages were for INH at 9 % and for RIF at 10 % while the overall NPs' yield reached only 30 %. The active ingredient concentration increases to 4 mg/mL reduced NPs sizes down to 257±4 nm while increasing loading efficiency of INH to 23 % and RIF to 20 % and resulting in a NPs yield of 37 %. The encapsulation process shows better performance at this additive concentration. The experimental system exhibits enhanced homogeneity as the concentration reaches 8 mg/mL where it maintains a stable particle size (266±1 nm) with lower polydispersity (0.196±0.061). This technique produces stable systems with high encapsulation by achieving both acceptable loading efficiency (INH 14 % and RIF 15 %) and maximum yield of NPs at 78 %. An increase in INH and RIF concentration to 10 mg/mL leads to reduced encapsulation (INH — 2 %, RIF — 3 %) along with decreased NP producing (18 %) even with small particle size (259±2 nm) and minimal polydispersity values (0.146±0.035). The drug substances tend to escape from the polymer matrix when it reaches saturation levels and leach into the surrounding aqueous solution which results in lower loading efficiency [22]. The formation of stable PLA nanoparticles reaches its optimal condition at INH and RIF concentration of 8 mg/mL since it creates ideal yield rates with suitable particle size distribution and drug loading efficiency.

The optimized nanoparticles exhibited optimal properties consisting of 197±8 nm average size and 0.287±0.048 polydispersity values and 23±2 % isoniazid loading efficiency alongside 20±8 % rifampicin loading efficiency and 65±2 % nanoparticle yield. Analysis of the produced nanoparticles included SEM examinations. Observations of Figure 2 indicate to the formation of round-shaped nanoparticles with a smooth surface. The software imageJ program enabled measurement of PLA-RIF-INH NPs size which amounted to 130±8 nm.

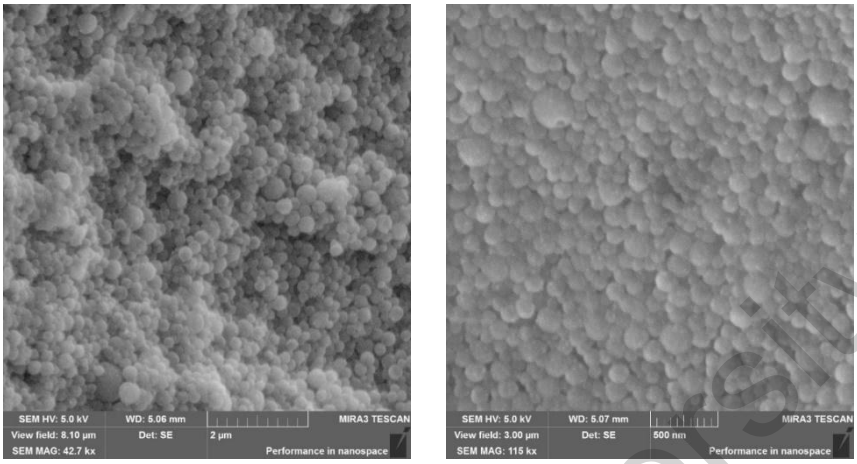


Figure 2. SEM images of PLA-RIF-INH NPs at a 2 µm and 500 nm scale

A zeta potential of PLA-RIF-INH NPs is +9.68±3 mV suggests that the nanoparticles possess a moderately positive surface charge, which is generally sufficient to maintain colloidal stability through electrostatic repulsion (Figure 3). Although higher absolute values (±30 mV or more) are typically associated with strongly stable systems, the observed value in this study was adequate to prevent aggregation under experimental conditions [23]. Moreover, the slightly positive charge may facilitate interaction with negatively charged components of bacterial cell walls or mucus layers, potentially enhancing cellular uptake and therapeutic efficacy.

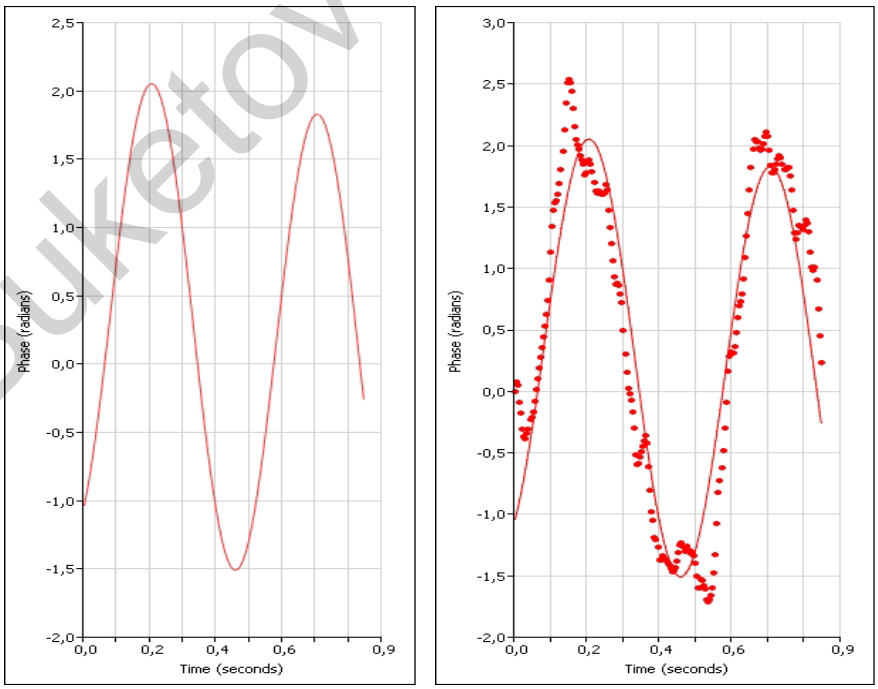


Figure 3. Zeta potential measurement of PLA-RIF-INH nanoparticles by phase analysis light scattering (PALS). The left panel shows the modeled phase shift curve, while the right panel displays experimental data (red dots) overlaid with the fitted curve

TGA and DSC were carried out to better understand the interaction of drugs with the polymer matrix of nanoparticles, and to confirm their effective incorporation into the structure (Figure 4).The study of thermal properties of isoniazid (Figure 4*a*) by DSC revealed a pronounced endothermic effect at 179.5 °C without mass loss, indicating a phase transition or melting of the substance [24, 25]. Thereafter, according to TGA, a gradual decrease in mass up to 25 % was observed in the temperature range of 250–450 °C, indicating thermal decomposition of the compound. The analysis of DSC and TGA curves of rifampicin (Figure 4*b*) demonstrates several peaks indicating the multistage character of the thermal decomposition of the drug substance. The first endothermic peak is observed at 188.7 °C and corresponds to the melting process of rifampicin. At this point, the substance passes from solid to liquid phase and no mass loss is recorded, indicating the absence of thermal decomposition. Then follows an exothermic peak at 209 °C, probably associated with the process of recrystallization and change of polymorphic form of rifampicin. This process is accompanied by partial decomposition of rifampicin with a mass loss of 10 %. The next exothermic peak at 253 °C is characterized by an additional 10 % mass loss, indicating the second stage of rifampicin decomposition [26]. The final stage of thermal decomposition is manifested by an exothermic peak at 425 °C, which is accompanied by a significant mass loss. The DSC curve of PLA (Figure 4*c*) shows a sharp endothermic peak at 330 °C, accompanied by a significant mass loss (up to 90 %), which indicates on intensive thermal decomposition of the polymer [3, 27]. The DSC curve of PLA nanoparticles encapsulated with isoniazid and rifampicin (Figure 4*d*) shows an endothermic peak at 350 °C, which is accompanied by thermal decomposition of the polymer matrix with a mass loss of 65 %. Compared to the DSC-curve of pure PLA, this peak has a lower intensity and is shifted to higher temperatures. This difference may indicate on a change in the thermal stability of PLA-INH-RIF nanoparticles, which may be the result of successful encapsulation of drugs and their interaction with the polymer matrix.

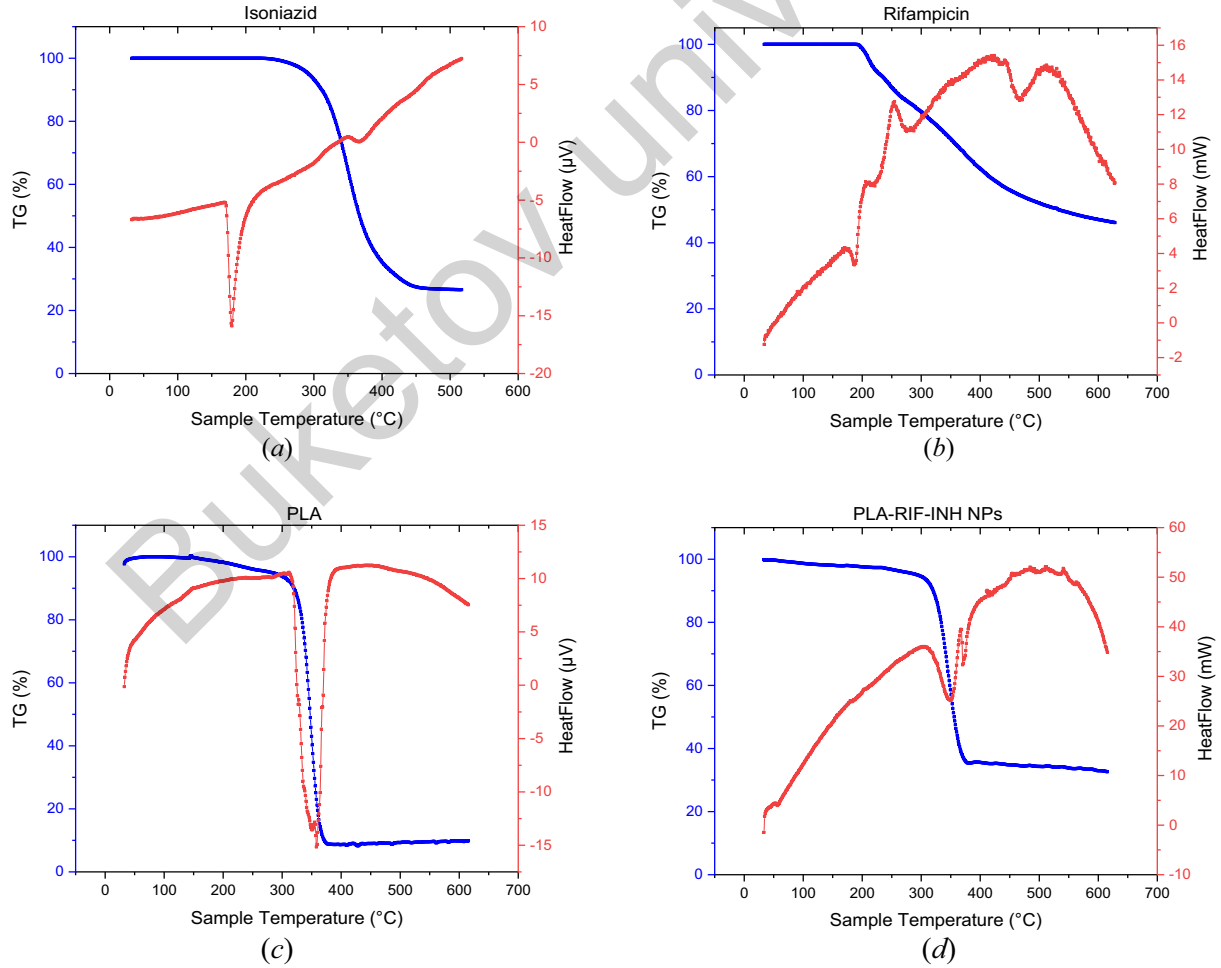


*a* — INH; *b* — RIF; *c* — PLA; *d* — PLA-RIF-INH NPs

Figure 4. Thermal properties of the system components and the synthesized nanoparticles

In this study, FTIR spectroscopy was used to characterize the individual components, as well as the synthesized PLA-RIF-INH nanoparticles (Figure 5). The FTIR spectrum of PLA shows a characteristic peak at 3395 $cm^{-1}$, which corresponds to valence vibrations of hydroxyl (–OH) groups present at the end of the polymer chain [28]. The band at 1705 $cm^{-1}$ corresponds to the valence vibrations of the carbonyl group (C=O). Asymmetric and symmetric vibrations of methyl groups ($–CH_3$) are observed at 2951 $cm^{-1}$ and 1361 $cm^{-1}$, respectively. The absorption at 1041 $cm^{-1}$ refers to the C-O bond vibrations. In addition, bending vibrations of $–CH_3$ asymmetric and symmetric type are identified at 1412 $cm^{-1}$ and 1361 $cm^{-1}$, respectively [3, 29]. The IR spectrum of INH shows characteristic absorption bands corresponding to its functional groups. The band at 3306 $cm^{-1}$ corresponds to the valence vibrations of the N–H bond. The band at 1670 $cm^{-1}$ indicates the presence of a carbonyl (C=O) group conjugated to the pyridine ring. The symmetric C=N stretching vibrations of the ring appear at 1554 $cm^{-1}$ while symmetric C=C stretching vibrations give rise to a peak at 1412 $cm^{-1}$ [30, 31]. The IR spectrum of RIF contains peaks which specifically identify the different functional groups within the molecule structure. N–H stretching occurs at 3418 $cm^{-1}$ thus verifying amino functional groups during analysis. The C–H bond shows valence vibrations that produce the signal at 2974 $cm^{-1}$. The carbonyl (C=O) group generates a peak at 1616 $cm^{-1}$ while C=C double bond vibrations correspond to the signal at 1454 $cm^{-1}$. The fundamental vibrational patterns of different rifampicin functional groups can be validated through peaks at 1381 $cm^{-1}$ ($CH_2$, C=C) and 1053 $cm^{-1}$ (–CH, CO, C–H) and 978 $cm^{-1}$ (≡C–H, C–H) [32–34].

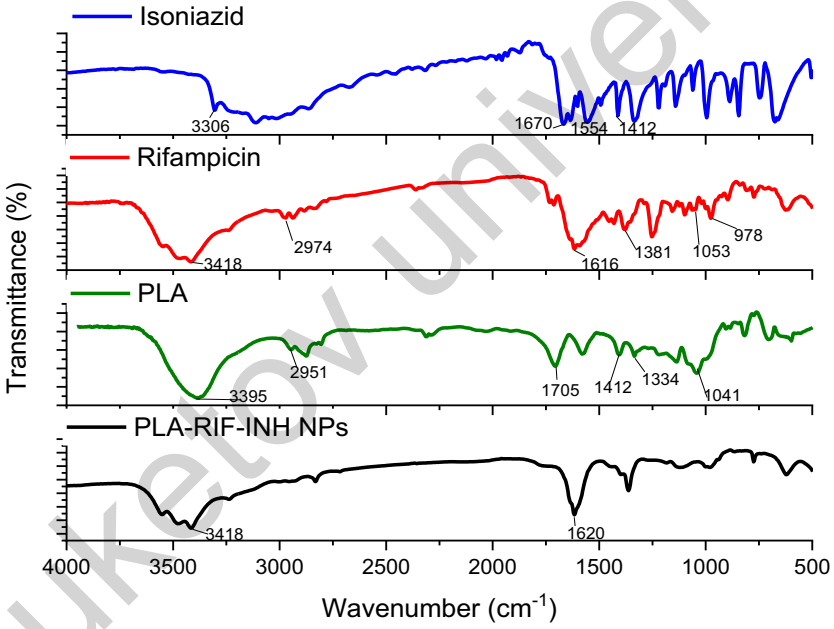


Figure 5. FTIR spectra for the system components and the synthesized nanoparticles

In the spectrum of the PLA-RIF-INH NPs the characteristic peaks of PLA, rifampicin, and isoniazid are still present, but with noticeable shifts and intensity changes. The broadening and slight shifts of the amide (1650 $cm^{-1}$) and hydroxyl (3400 $cm^{-1}$) peaks suggest hydrogen bonding interactions between the drugs and the PLA matrix. The ester peak of PLA at 1750 $cm^{-1}$ is retained, indicating that the polymer structure remains intact. However, the reduced intensity of the individual drug peaks suggests successful encapsulation and molecular interactions rather than simple physical mixing.

The release profiles of isoniazid and rifampicin from PLA-based nanoparticles were systematically evaluated *in-vitro* to understand the behavior of the drug under pH changes, which is very important for modeling physiological conditions in different parts of the body (Figure 6, 7). Different buffers were used to assess the impact of digestive tract conditions (acidic stomach pH 1.2 and neutral bloodstream pH 7.4, and slightly basic small intestine pH 6.8) on drug release from nanoparticles [35]. Two proven laboratory methods known as the Flow-Through Cell method (Sotax system) and the Franz diffusion cell method were used to evaluate the release kinetics. Both approaches offer distinct advantages and contribute to a comprehensive

analysis of drug release from PLA nanoparticles. Despite methodological differences, the drug release results demonstrated a 98 % correlation, confirming the reliability of the study and the appropriateness of the selected methods for achieving the research objectives.

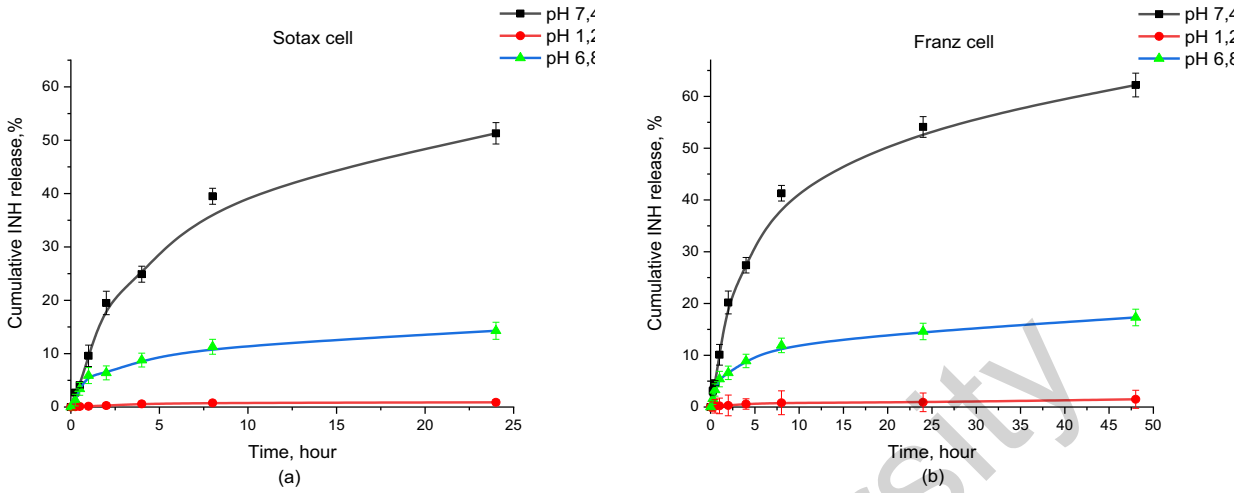


*a* — Sotax cell; *b* — Franz cell

Figure 6. Cumulative release of isoniazid from PLA-RIF-INH nanoparticles under different pH conditions using two release models

The graphs (Figure 6) show that the release of INH is strongly pH dependent. At pH 7.4, a significantly higher release of INH was observed in both dissolution systems. The release profile has a biphasic character, with an initial sharp release during the first few hours, followed by a slower, sustained release over time [36, 37]. This behavior suggests rapid diffusion of drug molecules adsorbed on the surface, followed by a more controlled release from the polymer matrix. The drug release rate showed reduced speed at pH 6.8 which demonstrates lower drug diffusion capability at these conditions. The extended drug release pattern shows that the polymer utilizes either breakdown processes or volume expansion to regulate delivery of medication. Under pH 1.2 conditions the INH release remained low for both nanoparticle systems proving their stability during exposure to strong acidic environments. Stability during oral drug delivery becomes vital since it ensures INH stays properly encapsulated throughout gastric transit towards its targeted site.

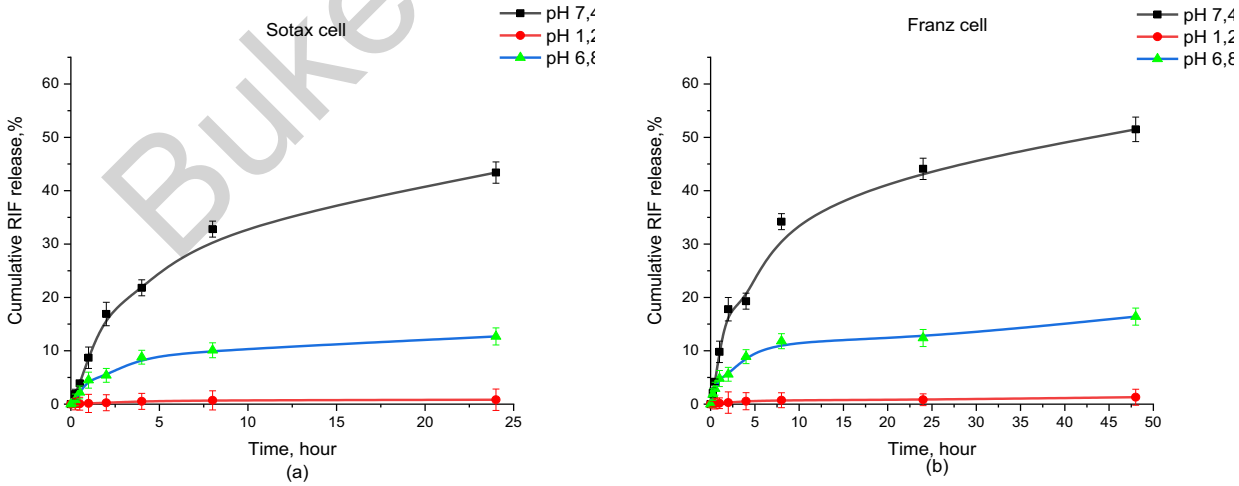


*a* — Sotax cell; *b* — Franz cell

Figure 7. Cumulative release of rifampicin from PLA-RIF-INH nanoparticles under different pH conditions using two release models

Analysis of rifampicin release profiles from PLA nanoparticles in Sotax and Franz cells at different pH values shows a clear dependence of dissolution kinetics on environmental conditions (Figure 7). In neutral medium, which mimics blood flow, the highest drug release is observed, reaching more than 43 % in 24 h in the Sotax system and more than 51.5 % in 48 h in the Franz cell, indicating good solubility of rifampicin under physiological conditions. In a slightly acidic medium (pH 6.8) corresponding to the intestine, the release was markedly lower but had a sustained and gradual pattern, confirming the potential of PLA nanoparticles for prolonged drug delivery. In acidic medium, simulating gastric conditions, rifampicin release was minimal, despite its relatively high solubility at this pH [38, 39].

The results show that PLA nanoparticles create an effective barrier for protected medications in acid environments and prolong their release at normal body pH levels essential for therapeutic effects. The PLA nanoparticle platform has demonstrated potential for tuberculosis treatment improvement through extended drug delivery at controlled rates and increasing bioavailability. This reduces the need for frequent dosing and minimizes side effects.

The antimycobacterial properties were evaluated for the PLA-RIF-INH NPs against PLA NPs without drug incorporation. Tests assessed the drug efficacy for three MTB strains which consisted of the drug-sensitive strain H37Rv in addition to isoniazid-resistant strain H and rifampicin-resistant strain R. The antimycobacterial effectiveness of developed nanoparticles was analyzed through medium Löwenstein-Jensen incubation for three weeks followed by Ziehl-Neelsen staining examination [17–19]. The concentration of the encapsulated drugs used in this study was 8 mg/mL for both rifampicin and isoniazid. Figure 8 shows how the bacterial growth changed after treatment with the nanoparticles. The graphs present the number of colony-forming units (CFU) per $10^7$ cells, comparing placebo PLA NPs with drug-loaded PLA-RIF-INH nanoparticles. In the H37Rv strain group, PLA-RIF-INH NPs markedly decreased the number of CFU compared to PLA NPs used as control, reflecting effective bacteriostatic activity. Similarly, a significant reduction in bacterial growth was observed for the H — strain, although slightly less than the drug-sensitive strain. A moderate reduction in CFU counts was also observed for the R strain group, reflecting the fact that encapsulation of RIF and INH in PLA NPs retains antimicrobial activity even for resistant strains.

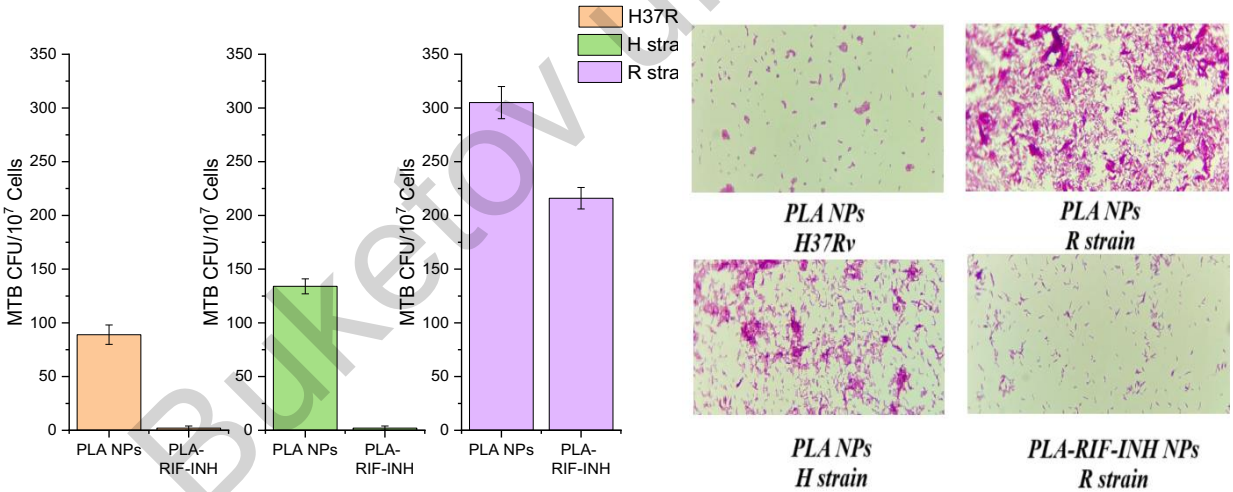


Figure 8. Antimycobacterial activity of PLA-RIF-INH NPs to different strains:
H37Rv, H strain — isoniazid-resistant strain, R strain — rifampicin-resistant strain

The microscopic image (Figure 8b) confirms bacterial growth in cultures which contained rifampicin-resistant strains. The nanoparticle formulation demonstrated strong suppression of isoniazid-sensitive MTB strains but showed restricted effectiveness against MTB strains resistant to rifampicin. The developed nanoparticles demonstrate potential for tuberculosis treatment by targeting isoniazid-resistant infections but more approaches are essential to address rifampicin resistance.

## *Conclusions*

The research developed and evaluated PLA NPs as drug carriers to deliver antituberculosis drugs including rifampicin and isoniazid. The optimized preparation method produced uniform PLA-RIF-INH NPs

with a 197±8 nm average diameter, 0.287±0.048 polydispersity index value, drug loading efficiency reaching 23±2 % isoniazid and 20±8 % rifampicin and a 65±2 % NPs yield. The use of the flow cell method and vertical diffusion technique in Franz cells evaluated rifampicin and isoniazid release from PLA NPs at gastrointestinal tract relevant pH values. Drug release shows its highest activity at pH 7.4 making this system suitable for systemic use. Studies using microbiological methods indicated that PLA-RIF-INH NPs exhibited antimycobacterial properties against sensitive Mycobacterium tuberculosis strain H37Rv as well as isoniazid-resistant H strain. The limited impact of the system on rifampicin-resistant strain R demonstrates the requirement to advance the composition and combination therapy strategies further. The developed PLA-RIF-INH NPs demonstrate potential as an effective tuberculosis medication delivery system by offering controlled drug release in conjunction with high effectiveness for both sensitive and isoniazid-resistant MTB strains. The study findings will serve as foundation data to enhance polymeric delivery system methods for tuberculosis treatment research.

*Supporting Information*

The Supporting Information is available free at https://ejc.buketov.edu.kz/index.php/ejc/article/view/272/215

*Funding*

This research was funded by the Science Committee of the Ministry of Science and Higher Education of the Republic of Kazakhstan under Grant No. AP14871344, titled "Development of colloidal biopolymer-based drug delivery systems for tuberculosis chemotherapy".

*Author Information**

**The authors' names are presented in the following order: First Name, Middle Name and Last Name*

**Aldana Rymzhanovna Galiyeva** (*corresponding author*) — Leading Researcher, Institute of Chemical Problems, Karaganda Buketov University, Universitetskaya street, 28, 100024, Karaganda, Kazakhstan; e-mail: aldana_karaganda@mail.ru; https://orcid.org/0000-0002-8551-6297

**Nazgul Asylbekkyzy Yessentayeva** — 3rd year PhD Student, Department of Organic Chemistry and Polymers, Karaganda Buketov University, Universitetskaya street, 28, 100024, Karaganda, Kazakhstan; e-mail: naz.yessentayeva92@gmail.com; https://orcid.org/0000-0003-4820-8460

**Dias Temirlanuly Marsel** — Master Student, Karaganda Buketov University, Universitetskaya street, 28, 100024, Karaganda, Kazakhstan.; e-mail: marsel.dias@bk.ru; https://orcid.org/0000-0002-1204-0814

**Arailym Turashkyzy Daribay** — Junior Researcher, Karaganda Buketov University, Universitetskaya street, 28, 100024, Karaganda, Kazakhstan; e-mail: arailymdaribay@gmail.com; https://orcid.org/0000-0001-5675-0351

**Daniyar Tleuzhanovich Sadyrbekov** — Candidate of Chemical Sciences, Researcher, Laboratory of the Engineering Profile "Physical and Chemical Methods of Research", Karaganda Buketov University, Universitetskaya street, 28, 100024, Karaganda, Kazakhstan; e-mail: daniyar81@gmail.com; https://orcid.org/0000-0002-3047-9142

**Rouslan Ibragimovich Moustafine** — Candidate of Science (Pharmacy), Associate Professor, Director of the Institute of Pharmacy, Kazan State Medical University, Fatykh Amirkhan Street, 16, 420126, Kazan, Russia; e-mail: ruslan.mustafin@kazangmu.ru, https://orcid.org/0000-0002-0916-2853

**Tatyana Valentinovna Kutulutskaya** — Head of the Laboratory of the "Regional Center of Phthisiopulmonology" of the Health Department of Karaganda region, Karaganda, Kazakhstan; e-mail: tata_kutul@mail.ru

References

1 Adepu, S., & Ramakrishna, S. (2021). Controlled Drug Delivery Systems: Current Status and Future Directions. *Molecules, 26*(19), 5905. https://doi.org/10.3390/molecules26195905

2 Liu, S., Qin, S., He, M., Zhou, D., Qin, Q., & Wang, H. (2020). Current applications of poly(lactic acid) composites in tissue engineering and drug delivery. *Composites Part B: Engineering, 199*, 108238. https://doi.org/10.1016/j.compositesb.2020.108238

3 Galiyeva, A., Daribay, A., Tabriz, N., & Tazhbayev, Y. (2024). Production of Polylactide Nanoparticles Loaded With Isoniazid and Vitamin C: A Promising Candidate for the Treatment of Resistant Forms of Tuberculosis. *Journal of Polymer Science. Portico, 1–11*. https://doi.org/10.1002/pol.20240375

4 Tazhbayev, Y., Burkeyev, M., Zhaparova, L., Zhumagalieva, T., & Arystanova. (2018). Nanoparticles on the basis of polylactic acid and polylactic-co-glycolic acids loaded with drugs. *Bulletin of the Karaganda University. "Chemistry" Series, 90*(2), 31–39. https://doi.org/10.31489/2018ch2/31-39

5 Bakare, A.A., Moses, V.Y., Beckely, C.T., Oluyemi, T.I., Ogunfeitimi, G.O., Adelaja, A.A., Ayorinde, G.T., Gbadebo, A.M., Fagbenro, O.S., Ogunsuyi, O.I., Ogunsuyi, O.M., & Ige, O.M. (2022). The first-line antituberculosis drugs, and their fixed-dose combination induced abnormal sperm morphology and histological lesions in the testicular cells of male mice. *Frontiers in Cell and Developmental Biology*, 10. https://doi.org/10.3389/fcell.2022.1023413

6 Srivastava, S., Sherman, C., Meek, C., Leff, R., & Gumbo, T. (2011). Pharmacokinetic Mismatch Does Not Lead to Emergence of Isoniazid- or Rifampin-Resistant Mycobacterium tuberculosis but to Better Antimicrobial Effect: a New Paradigm for Antituberculosis Drug Scheduling. *Antimicrobial Agents and Chemotherapy, 55*(11), 5085–5089. https://doi.org/10.1128/aac.00269-11

7 Galiyeva, A., Daribay, A., Zhumagaliyeva, T., Zhaparova, L., Sadyrbekov, D., &Tazhbayev, Y. (2023). Human Serum Albumin Nanoparticles: Synthesis, Optimization and Immobilization with Antituberculosis Drugs. *Polymers, 15*(13), 2774. https://doi.org/10.3390/polym15132774

8 Pienaar, E., Linderman, J.J., & Kirschner, D.E. (2018). Emergence and selection of isoniazid and rifampin resistance in tuberculosis granulomas. *PLOS ONE, 13*(5), e0196322. https://doi.org/10.1371/journal.pone.0196322

9 Lee, B.K., Yun, Y., & Park, K. (2016). PLA micro- and nano-particles. *Advanced Drug Delivery Reviews, 107*, 176–191. https://doi.org/10.1016/j.addr.2016.05.020

10 Pulingam, T., Foroozandeh, P., Chuah, J.-A., & Sudesh, K. (2022). Exploring Various Techniques for the Chemical and Biological Synthesis of Polymeric Nanoparticles. *Nanomaterials, 12*(3), 576. https://doi.org/10.3390/nano12030576

11 Li, Y., Zhang, L., Tian, R., Pranantyo, D., Chen, L., & Xia, F. (2023). A Double-Emulsion Method for the Fabrication of PLA Single-Hole HollowParticles. *Current Chinese Science, 3*(4), 285–292. https://doi.org/10.2174/2210298103666230428092735

12 Sarsenbekova, A.Zh., Bolatbay, A.N., Morgun, V.V., Havlicek, D., Davrenbekov, S.Zh., & Nasikhatuly, E. (2022). Study of thermal stability and determination of effective activation energy values during degradation of unsaturated polyester copolymers atmosphere. *Bulletin of the University of Karaganda — Chemistry, 105*(1), 86–91. https://doi.org/10.31489/2022Ch1/86-91

13 Burkeyev, M., Tazhbayev, Y., Bolatbay, A., Minayeva, Y., Davrenbekov, S., Nassikhatuly, Y., Kovaleva, A., Kutzhanova, K., & Kazhmuratova, A. (2022). Study of Thermal Decomposition of the Copolymer Based on Polyethylene Glycol Fumarate with Acrylic Acid. *Journal of Chemistry, 2022*, 514358. https://doi.org/10.1155/2022/3514358

14 Sarsenbekova, A.Zh., Bolatbay, A.N., Havlicek, D., Issina, Zh.A., Sarsenbek, A.Zh., Kabdenova, N.A., & Kilybay, M.A. (2024). Effect of Heat Treatment on the Supramolecular Structure of Copolymers Based on Poly(propylene glycol fumarate phthalate) with Acrylic Acid. *Eurasian Journal of Chemistry, 29*(2), 114, 61–73. https://doi.org/10.31489/2959-0663/2-24-9

15 Borsynbayev, A., Omarov, K., Mustafin, Y., Havlícek, D., Absat, Z., Muratbekova, A., Kaikenov, D., Pudov, A., & Shuyev, N. (2022). A study of copper leaching from the tailings of the Karagaily (Republic of Kazakhstan) concentrating factory using an electric hydropulse discharge. *Journal of the Serbian Chemical Society, 87*(7-8), 925–937. https://doi.org/10.2298/JSC2208925B

16 Saranjit, S., Mariappan, T.T., Sharda, N., & Singh, B. (2000). Degradation of Rifampicin, Isoniazid and Pyrazinamide from Prepared Mixtures and Marketed Single and Combination Products Under Acid Conditions. *Pharmacy and Pharmacology Communications, 6*(11), 491–494. https://doi.org/10.1211/146080800128735575

17 Hakkimane, S., Shenoy, V.P., Gaonkar, S., Bairy, I., & Guru, B.R. (2018). Antimycobacterial susceptibility evaluation of rifampicin and isoniazid benz-hydrazone in biodegradable polymeric nanoparticles against Mycobacterium tuberculosis H37Rv strain. *International Journal of Nanomedicine, 13*, 4303–4318. https://doi.org/10.2147/ijn.s163925

18 Heidary, M., Zaker Bostanabad, S., Amini, S.M., Jafari, A., Ghalami Nobar, M., Ghodousi, A., Kamalzadeh, M., & Darban-Sarokhalil, D. (2019). The anti-mycobacterial activity of Ag, ZnO, and Ag-ZnO nanoparticles against MDR- and XDR-Mycobacterium tuberculosis strains. *Infection and Drug Resistance, 12*, 3425–3435. https://doi.org/10.2147/idr.s221408

19 Van Deun, A., Hossain, M.A., Gumusboga, M., & Rieder, H.L. (2008). Ziehl-Neelsen staining: theory and practice. *The International Journal of Tuberculosis and Lung Disease, 12*(1), 108–110.

20 Dzodanu, E.G., Afrifa, J., Acheampong, D.O., & Dadzie, I. (2019). Diagnostic yield of fluorescence and Ziehl-Neelsen staining techniques in the diagnosis of pulmonary tuberculosis: A comparative study in a district health facility. *Tuberculosis Research and Treatment, 2019*, 4091937. https://doi.org/10.1155/2019/4091937

21 Lagreca, E., Onesto, V., Di Natale, C., La Manna, S., Netti, P.A., & Vecchione, R. (2020). Recent advances in the formulation of PLGA microparticles for controlled drug delivery. *Progress in Biomaterials, 9*(4), 153–174. https://doi.org/10.1007/s40204-020-00139-y

22 Galiyeva, A.R., Tazhbayev, Ye.M., Zhumagaliyeva, T.S., Sadyrbekov, D.T., Kaikenov, D.A., Karimova, B.N., & Shokenova, S.S. (2022). Polylactide-co-glycolide nanoparticles immobilized with isoniazid: optimization using the experimental Taguchi method. *Bulletin of the Karaganda University. "Chemistry" Series, 105*(1), 69–77. https://doi.org/10.31489/2022ch1/69-77

23 Basílio, J.A.J., & Shinde, M.D. (2024). Colloidal stability and dielectric behavior of eco-friendly synthesized zinc oxide nanostructures from Moringa seeds. *Scientific Reports, 14*, 2310. https://doi.org/10.1038/s41598-024-52093-5

24 Galiyeva, A.R., Tazhbayev, Y.M., Yessentayeva, N.A., Daribay, A.T., Marsel, D.T., Sadyrbekov, D.T., Zhaparova, L.Zh., & Arystanova, Z.T. (2023). PEGylation of Albumin Nanoparticles Immobilized with the Anti-Tuberculosis Drug "Isoniazid." *Eurasian Journal of Chemistry, 110*(2), 42–50. https://doi.org/10.31489/2959-0663/2-23-7

25 Tazhbayev, Ye.M., Galiyeva, A.R., Zhumagaliyeva, T.S., Burkeyev, M.Zh., Kazhmuratova, A.T., Zhakupbekova, E.Zh., Zhaparova, L.Zh., & Bakibayev, A.A. Synthesis and characterization of isoniazid immobilized polylactide-co-glycolide nanoparticles. *Bulletin of the University of Karaganda — Chemistry, 101*(1), 61–70. https://doi.org/10.31489/2021Ch1/61-70

26 Alves, R., Reis, T.V. da S., Silva, L.C.C. da, Storpírtis, S., Mercuri, L.P., & Matos, J. do R. (2010). Thermal behavior and decomposition kinetics of rifampicin polymorphs under isothermal and non-isothermal conditions. *Brazilian Journal of Pharmaceutical Sciences, 46*(2), 343–351. https://doi.org/10.1590/s1984-82502010000200022

27 W. Badri, K. Miladi, Q.A. Nazari, H. Fessi, & A. Elaissari (2017). "Effect of Process and Formulation Parameters on Polycaprolactone Nanoparticles Prepared by Solvent Displacement," *Colloids and Surfaces A: Physicochemical and Engineering Aspects, 516*, 238–244, https://doi.org/10.1016/j.colsu rfa.2016.12.029

28 Symons, A.L., Varanasi, S., Fredericks, P.M., Whittaker, A.K., Hill, D.J.T., & Rasoul, F. (2013). FT-IR characterization and hydrolysis of PLA-PEG-PLA based copolyester hydrogels with short PLA segments and a cytocompatibility study. *Journal of Polymer Science Part A: Polymer Chemistry, 51*(24), 5163–5176. https://doi.org/10.1002/pola.26930

29 Chieng, B., Ibrahim, N., Yunus, W., & Hussein, M. (2013). Poly(lactic acid)/Poly(ethylene glycol) Polymer Nanocomposites: Effects of Graphene Nanoplatelets. *Polymers, 6*(1), 93–104. https://doi.org/10.3390/polym6010093

30 Tazhbayev, Y., Galiyeva, A., Zhumagaliyeva, T., Burkeyev, M., & Karimova, B. (2021). Isoniazid—Loaded Albumin Nanoparticles: Taguchi Optimization Method. *Polymers, 13*(21), 3808. https://doi.org/10.3390/polym13213808

31 Gunasekaran, S., Sailatha, E., Seshadri, S., & Kumaresan, S. (2009). FTIR, FT Raman spectra and molecular structural confirmation of isoniazid. *Indian Journal of of Pure & Applied Physics, 47,* 12–18.

32 Sharma, A., Puri, V., Kumar, P., Singh, I., & Huanbutta, K. (2021). Development and Evaluation of Rifampicin Loaded Alginate–Gelatin Biocomposite Microfibers. *Polymers, 13*(9), 1514. https://doi.org/10.3390/polym13091514

33 Ivashchenko, O., Tomila, T., Ulyanchich, N., Yarmola, T., & Uvarova, I. (2014). Fourier-Transform Infrared Spectroscopy of Antibiotic Loaded Ag-Free and Ag-Doped Hydroxyapatites. Advanced Science, *Engineering and Medicine, 6*(2), 193–202. https://doi.org/10.1166/asem.2014.1473

34 Yessentayeva, N.A., Galiyeva, A.R., Daribay, A.T., Sadyrbekov, D.T., Moustafine, R.I., & Tazhbayev, Y.M. (2024). Optimization of Polylactide-Co-Glycolide-Rifampicin Nanoparticle Synthesis, In Vitro Study of Mucoadhesion and Drug Release. *Polymers, 16*(17), 2466. https://doi.org/10.3390/polym16172466

35 Galiyeva, A.R., Tazhbayev, Ye.M., Zhumagaliyeva, T.S., & Daribay, A.T. (2022). Encapsulation of Isoniazid in Polylactide-Co-Glycolide Nanoparticles by Nanoprecipitation. *Bulletin of the University of Karaganda — Chemistry, 107*(3), 208–217. https://doi.org/10.31489/2022Ch3/3-22-17

36 Chorny, M., Fishbein, I., Danenberg, H.D., & Golomb, G. (2002). Lipophilic drug loaded nanospheres prepared by nanoprecipitation: effect of formulation variables on size, drug recovery and release kinetics. *Journal of Controlled Release, 83*(3), 389–400. https://doi.org/10.1016/s0168-3659(02)00211-0

37 Loiko, O.P., Herk, A.M. van, Ali, S.I., Burkeev, M.Zh., Tazhbayev, Y.M., & Zhaparova, L.Zh. (2013). Controlled release of Capreomycin sulfate from pHresponsive nanocapsules. *E-Polymers, 13*(1). https://doi.org/10.1515/epoly-2013-0118

38 Gao, Y., Zuo, J., Bou-Chacra, N., Pinto, T. de J.A., Clas, S.-D., Walker, R.B., & Löbenberg, R. (2013). In Vitro Release Kinetics of Antituberculosis Drugs from Nanoparticles Assessed Using a Modified Dissolution Apparatus. *BioMed Research International, 2013, 1–9*. https://doi.org/10.1155/2013/136590

39 Arca, H.Ç., Mosquera-Giraldo, L.I., Pereira, J.M., Sriranganathan, N., Taylor, L.S., & Edgar, K.J. (2018). Rifampin Stability and Solution Concentration Enhancement Through Amorphous Solid Dispersion in Cellulose ω-Carboxyalkanoate Matrices. *Journal of Pharmaceutical Sciences, 107*(1), 127–138. https://doi.org/10.1016/j.xphs.2017.05.036